EurJIC European Journal of Inorganic Chemistry

ChemPubSoc Europe

FULL PAPER

DOI:10.1002/ejic.201500351

A Heterodinuclear $Fe^{III}Zn^{II}$ Complex as a Mimic for Purple Acid Phosphatase with Site-Specific Zn^{II} Binding

Asha E. Roberts,[a] Gerhard Schenk,[a] and Lawrence R. Gahan*[a]

Keywords: Bioinorganic chemistry / Biomimetic synthesis / Enzyme models / Purple acid phosphatase / Phosphodiester-degrading enzyme

Purple acid phosphatases (PAPs) are the only dinuclear metallohydrolases for which the necessity for a heterovalent active site (Fe^{III}–M^{II}; M = Fe, Zn or Mn) for catalysis has been established. A major goal for the synthesis of PAP biomimetics is to design a ligand in which the two coordination sites exhibit discrimination between the trivalent and divalent metal ions. With this goal in mind the ligand 2-{[bis(2-methoxyethyl)amino]methyl}-6-{[(2-hydroxybenzyl)(2-pyridylmethyl)amino]methyl}-4-methylphenol ($BMMHPH_2$), with two distinct coordination sites, N_2O_2 (α) and NO_3 (β), has been prepared. Although not exactly mimicking the active site of PAP, the ligand facilitated the formation of the complex $[Fe^{III}Zn^{II}(BMMHP)(CH_3COO)_2](BPh_4)$, which exhibited regioselectivity in the two metal binding sites. The phosphoesterase-like activity of the complex in 50:50 acetonitrile/water was investigated by using the substrate bis(2,4-dinitrophenyl) phosphate (BDNPP) yielding kinetically relevant pK_a values of 6.89, 7.37 and 9.00, a K_M of 10.8 ± 2.1 mM and a k_{cat} of $3.20 \pm 0.38 \times 10^{-3}$ s^{-1} (at pH = 7.5). Attempts to prepare a diiron analogue resulted in a centrosymmetric dimer, $[Fe^{III}_2(BMMHPH)_2(\mu\text{-}OH)_2](BPh_4)_2$, with one six-coordinate Fe^{III} atom in each of the α-sites, connected by two μ-hydroxido groups. In this $Fe(\mu\text{-}OH)_2Fe$ diamond core the Fe^{III} ions are weakly antiferromagnetically coupled, with $J = -1.76 \pm 0.03$ cm^{-1}. The β-sites were vacant. Attempts to replace the Zn^{II} ion with Mg^{II} resulted in the formation of a centrosymmetric trimer, i.e. $[Fe^{III}_2Mg^{II}(BMMHPH)_2(CH_3COO)_2(CH_3O)_2](BPh_4)_2$.

Introduction

Purple acid phosphatase (PAP), a monophosphoesterase within the dinuclear metallohydrolase family, has been isolated from porcine uterine fluid,[1] bovine spleen,[2] red kidney beans,[3] tomatoes,[4] sweet potatoes,[5] soybeans,[6] rice,[7] humans[8] and rats.[9] The precise physiological role of PAP is still not well understood; however, studies have linked the enzyme to several functions in both mammals and plants. Most notably, in mammals the maintenance of normal bone turnover by PAP has made it a potential drug target for treating osteoporosis.[10]

Because of the complexity and large size of PAP, the development of simpler synthetic models is instructive in understanding its mechanistic properties.[10,11] Challenges in the design and synthesis of such models are not only encountered in replicating the distinct enzymatic coordination environment, but also in providing regioselectivity with respect to metal ion binding.[12] Site-specific metal ion binding is often inferred by reference to differences in bond lengths and anticipated hard/soft binding preferences of each metal ion. The possibility of a reversed or disordered occupancy is often not considered, even in cases where the metal ions are added simultaneously. A clear demonstration of regioselectivity can be achieved by the isolation and crystallographic characterisation of a mononuclear complex, showing discrimination between the two sites and allowing for controlled, stepwise preparation of the heterodinuclear complex.[12a,12g,13] A number of examples of the types of ligands previously employed in these studies is given in Figure 1. Ligand (a), 2-{[bis(pyridin-2-ylmethyl)amino]methyl}-6-{[(2-hydroxybenzyl)(pyridin-2-ylmethyl)amino]methyl}-4-methylphenol ($BPBPMPH_2$),[12c,12d,14] was one of the first ligands reported, which replicated the structural and functional features of the active site of PAP. Other ligands shown in Figure 1 illustrate attempts to replicate the regioselectivity observed in PAP through either design or complexation approaches. For example, ligand (c) was isolated as a ferrous complex with the Fe^{III} ion binding to the N_3O site, leaving the N_2O_2 site open for a divalent metal ion.[13a] Conversely, isolation of ligand (d) as a mononuclear complex with either Cu^{II} or Zn^{II} residing in the N_3O site has also been reported.[12g,13b] More recently, ligands (e) and (f) have been isolated with Fe^{III} selectively coordinated to the N_2O_2 sites, with subsequent addition of Zn^{II} to the N_2O site.[12a] Notably, these last two complexes, when left to stand in basic aqueous solution, decomposed to form dizinc complexes after 1 d.[12a]

[a] School of Chemistry and Molecular Biosciences, TheUniversity of Queensland, Brisbane, Queensland 4072, Australia
E-mail: gahan@uq.edu.au
http://staff.scmb.uq.edu.au/staff/gary-schenk
http://staff.scmb.uq.edu.au/staff/lawrence-gahan

Supporting information for this article is available on the WWW under http://dx.doi.org/10.1002/ejic.201500351.

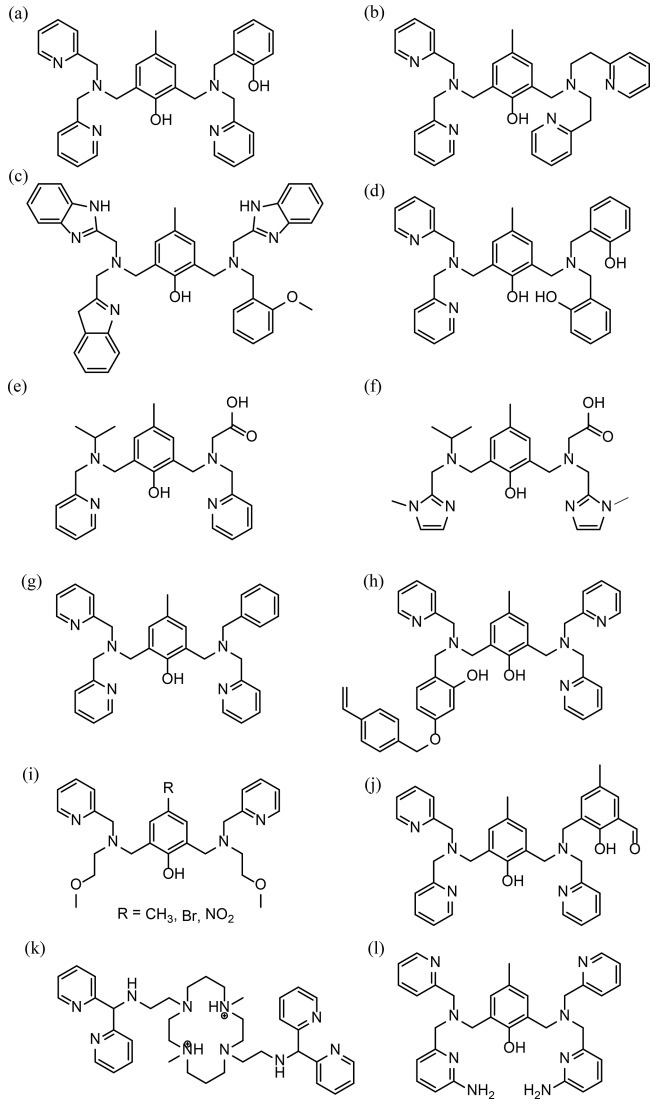

Figure 1. Examples of dinucleating ligands for the synthesis of heterodinuclear complexes as structural models of PAP: (a),[12c,12d,12m–12o,12q] (b),[44] (c),[13a] (d),[12g,13b] (e),[12a] (f),[12a,42] (g),[23e] (h),[12i] (i),[23d] (j),[12b,19] (k),[11a] (l).[11c]

In the present study we focus on the dinucleating asymmetric ligand 2-{[bis(2-methoxyethyl)amino]methyl}-6-{[(2-hydroxybenzyl)(2-pyridylmethyl)amino]methyl}-4-methylphenol ($BMMHPH_2$) (Figure 2), which has been designed

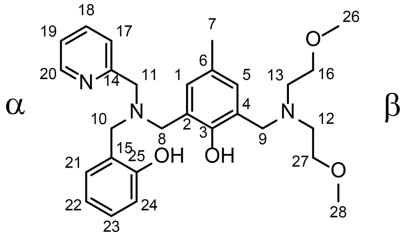

Figure 2. Dinucleating asymmetric ligand, 2-{[bis(2-methoxyethyl)-amino]methyl}-6-{[(2-hydroxybenzyl)(2-pyridylmethyl)amino]-methyl}-4-methylphenol ($BMMHPH_2$) (the numbers refer to the NMR assignments described in the Experimental Section).

with two distinct coordination sites, N_2O_2 (α) and NO_3 (β). While Fe^{III} has been reported to bind to the α-site[15] it was anticipated that the poor electron-donating properties of the β-site would exhibit reduced Fe^{III} binding affinity and permit regioselective binding of Zn^{II} to this β-site. In a further study we attempted to replace Zn^{II} with Mg^{II}, according to recent proposals that Mg^{II} could effectively replace Zn^{II}, and other metal ions, in corresponding hydrolytic enzymes.[16]

Results and Discussion

Synthesis of Ligands and Complexes

The ligand 2-{[bis(2-methoxyethyl)amino]methyl}-6-{[(2-hydroxybenzyl)(2-pyridylmethyl)amino]methyl}-4-methylphenol ($BMMHPH_2$) was prepared according to a statistical methodology by reaction between (2-hydroxybenzyl)(2-pyridylmethyl)amine[17] (HBPA), 2,6-bis(chloromethyl)-4-methylphenol[18] and bis(2-methoxyethyl)amine in THF solution in the presence of base. The desired ligand was isolated after column chromatography and characterized by IR and NMR spectroscopy as well as mass spectrometry. The ligand nomenclature for $BMMHPH_2$ follows that employed for this type of ligands and implies that the two phenol groups are protonated; when coordinated, the ligand can be doubly deprotonated ($BMMHP^{2-}$) or protonated at one site ($BMMHPH^{-}$), usually at a tertiary amine (vide infra).

Reaction of the ligand with iron(II) acetate and zinc(II) acetate resulted in the isolation of $[Fe^{III}Zn^{II}(BMMHP)(CH_3COO)_2](BPh_4)$ after addition of sodium tetraphenylborate. In an effort to prepare the Fe^{III}/Fe^{II} or Fe^{III}/Fe^{III} analogues, the ligand was treated with iron(II) acetate resulting in the isolation of a complex subsequently characterized as $[Fe^{III}_2(BMMHPH)_2(\mu\text{-}OH)_2](BPh_4)_2$. Reaction with magnesium(II) acetate in place of the zinc(II) acetate in an attempt to prepare $[Fe^{III}Mg^{II}(BMMHP)(CH_3COO)_2](BPh_4)$ and thus examine the suggested utility of Mg^{II} in these phosphatase mimics,[16] resulted in the complex $[Fe^{III}_2Mg^{II}(BMMHPH)_2(CH_3COO)_2(CH_3O)_2](BPh_4)_2$. The three complexes have been characterized by X-ray crystallography; the magnetic susceptibility properties of $[Fe^{III}_2(BMMHPH)_2(\mu\text{-}OH)_2](BPh_4)_2$ have been measured, and the hydrolytic activity of $[Fe^{III}Zn^{II}(BMMHP)(CH_3COO)_2](BPh_4)$ and $[Fe^{III}_2(BMMHPH)_2(\mu\text{-}OH)_2](BPh_4)_2$ with the activated substrate bis(2,4-dinitrophenyl) phosphate (BDNPP) has been determined.

Solid-State Structures

Crystal structures of the complexes characterised as $[Fe^{III}Zn^{II}(BMMHP)(CH_3COO)_2](BPh_4)$, $[Fe^{III}_2(BMMHPH)_2(\mu\text{-}OH)_2](BPh_4)_2$ and $[Fe^{III}_2Mg^{II}(BMMHPH)_2(CH_3COO)_2(CH_3O)_2](BPh_4)_2$ were obtained. The three structures are presented in Figures 3, 4, and 5, respectively,

and the X-ray crystal data are presented in Table S1. Selected bond lengths and angles are presented in Tables S2–S4.

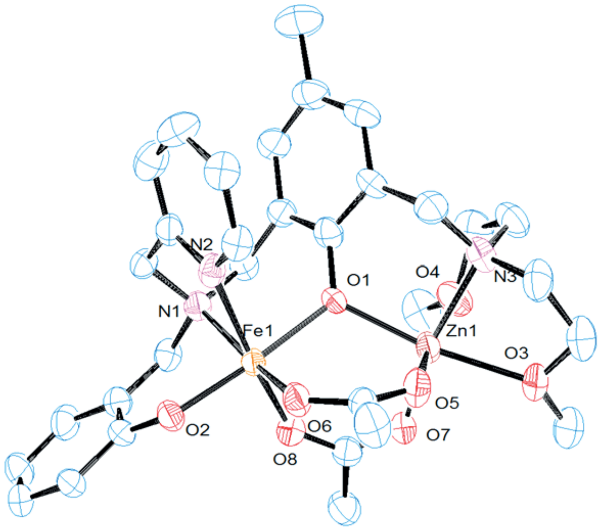

Figure 3. ORTEP plot of $[Fe^{III}Zn^{II}(BMMHP)(CH_3COO)_2](BPh_4)$. Hydrogen atoms, counterion and labels of non-coordinating atoms have been omitted for clarity.

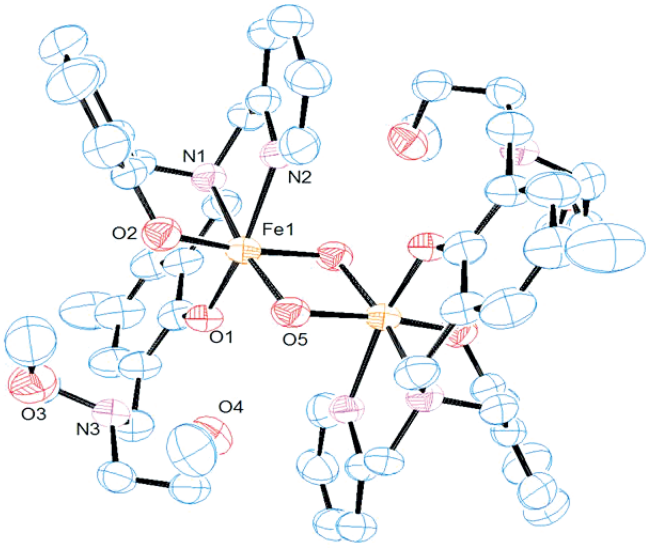

Figure 4. ORTEP plot of $[Fe^{III}_2(BMMHPH)_2(\mu\text{-}OH)_2](BPh_4)_2$. Hydrogen atoms, counterions and labels of non-coordinating atoms have been omitted for clarity.

The X-ray structure of $[Fe^{III}Zn^{II}(BMMHP)(CH_3COO)_2](BPh_4)$ consists of one ligand with a hexacoordinate metal atom (Fe^{III} and Zn^{II}) in each site, two bridging acetates, and one tetraphenylborate counterion. The bond lengths of Fe(1) with O(1), O(2), N(1) and N(2) of the α-site are within the usual range for Fe^{III} in this coordination environment.[12b–12d,12m–12r,19] Both Fe–N bonds are significantly longer than the Fe–O bonds with an average difference of 0.221 Å. Bond lengths of each metal with the bridging oxygen donors [O(1), O(5)/(6), O(7)/(8)] show the Fe bonds to

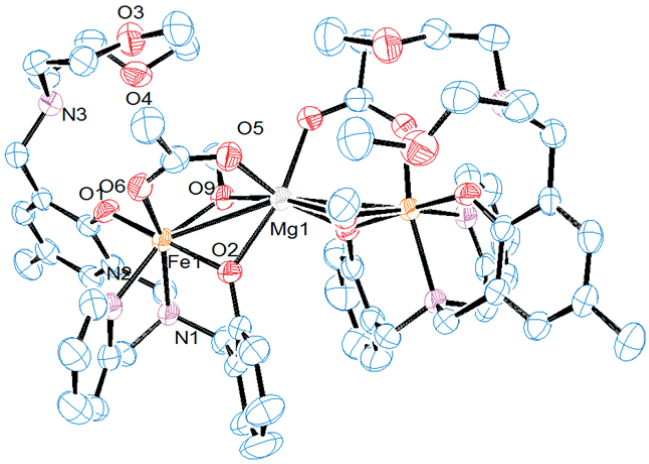

Figure 5. ORTEP plot of $[Fe^{III}_2Mg^{II}(BMMHPH)_2(CH_3COO)_2(CH_3O)_2](BPh_4)_2$. Hydrogen atoms, counterions and labels of non-coordinating atoms have been omitted for clarity.

be slightly shorter than the corresponding Zn bonds. In both cases the carboxyl oxygen atoms *trans* to the coordinated amines [N(1) and N(3)] have bonds slightly shorter than the neighbouring carboxyl oxygen atom. The longer bonds between Zn(1) and the two ether oxygen donors, O(3) and O(4), of the β-site are within the range of Zn^{II}–ether bonds found in similar models,[20] and the difference in lengths between the axial [O(4)] and equatorial [O(3)] positions is also a common observation.[20b,20c,21] The crystal structure of $[Fe^{III}Zn^{II}(BMMHP)(CH_3COO)_2](BPh_4)$ was solved with the two metal ions exchanged and disordered between the two sites but resulted in *R* factors larger than 10%. Solving the structure as an $Fe^{III}Fe^{II}$ complex gave a fit similar to that of the $Fe^{III}Zn^{II}$ complex. However, mass spectrosmetric data (vide infra) and elemental Fe and Zn analyses revealed the complex to contain iron and zinc in a 1:1 ratio. The Fe(1)···Zn(1) separation of 3.421 Å is comparable to that of the native enzyme in the presence of bound phosphate (3.33 Å).[22] However, it is important to note that under kinetic conditions (50:50 acetonitrile/water) the acetates are exchanged for a bridging hydroxido group, and the Fe(1)···Zn(1) separation is expected to be reduced by ca. 0.45 Å.[12c,12d] Nonetheless, the structure of $[Fe^{III}Zn^{II}(BMMHP)(CH_3COO)_2](BPh_4)$ is comparable to previously reported biomimetics of PAP and related metallohydrolases indicating that it is a practical structural model for the enzyme.[12b–12e,12m–12r,17,19,23]

The X-ray structure of $[Fe^{III}_2(BMMHPH)_2(\mu\text{-}OH)_2](BPh_4)_2$ indicates that the molecule consists of a centrosymmetric dimer, comprised of two ligands, one six-coordinate Fe^{III} atom in each α-site, two μ-hydroxido groups and two tetraphenylborate counterions. The β-sites are unoccupied, with the tertiary amines protonated. Repeated attempts to prepare a di-Fe^{III} or $Fe^{III}Fe^{II}$ complex with the metal ions in the respective α- and β-sites resulted in the same centrosymmetric dimer, suggesting strongly that the methoxy donors have very little affinity to Fe^{III} or Fe^{II}. The Fe(μ-OH)$_2$Fe diamond core has an Fe^{III}···Fe^{III} distance of

3.103 Å and an O(5)–Fe(1)–O(5)* angle of 79.46(13)°. The Fe(1)–O(5)–Fe(1)* angle of 100.54(13)° is slightly smaller in comparison to similar diamond-core complexes.[24] As is commonly observed in diiron diamond cores,[24b,25] the Fe–O distances are not identical, instead there are two sets of Fe^{III}–O bond lengths, 1.980(4) and 2.054(3). Unlike the $[Fe^{III}Zn^{II}(BMMHP)(CH_3COO)_2](BPh_4)$ structure the Fe(1) distances between the two phenolate oxygen atoms [O(1) and O(2)] are similar. The Fe(1)–N distances with the tertiary amine [N(1)] and pyridine [N(2)] are, however, similar to those of $[Fe^{III}Zn^{II}(BMMHP)(CH_3COO)_2](BPh_4)$.

The X-ray crystal structure of the third complex was solved as a centrosymmetric $Fe^{III}{}_2Mg^{II}$ trimer, $[Fe_2Mg(BMMHPH)_2(CH_3COO)_2(CH_3O)_2](BPh_4)_2$. The structure is comprised of two ligands, one Fe^{III} atom in each α-site and an Mg^{II} atom linking the two Fe^{III} centres. The Mg^{II} ion is bridged to both Fe^{III} ions by an acetate [O(5)/(6)], a methoxide [O(9)] and the terminal phenolate [O(2)] of the α-site. All three centres are hexacoordinate. The β-sites are unoccupied with protonation of the tertiary amines. Mg(1) lies directly in the centre of symmetry, and the Fe(1)···Mg(1) distance is 3.0266(6) Å. The Fe(1)–O(2) bond of the terminal phenolate is slightly longer than in the structures of $[Fe^{III}Zn^{II}(BMMHP)(CH_3COO)_2](BPh_4)$ and $[Fe^{III}{}_2(BMMHPH)_2(\mu\text{-}OH)_2](BPh_4)_2$, in which bridging by this donor ligand does not occur. The Fe(1)–O distance with each bridging oxygen atom is shorter than the corresponding Mg(1)–O distances by about 0.05, 0.09 and 0.1 Å for the bridging acetate [O(5)/(6)], phenolate [O(2)] and methoxide [O(9)], respectively.

Infrared Spectroscopy

The IR spectra of both $[Fe^{III}Zn^{II}(BMMHP)(CH_3COO)_2](BPh_4)$ and $[Fe^{III}{}_2Mg^{II}(BMMHPH)_2(CH_3COO)_2(CH_3O)_2](BPh_4)_2$ exhibit bands associated with coordinated acetates (ν_{asym} = 1589, 1582 cm^{-1} and ν_{sym} = 1424, 1430 cm^{-1}, respectively). The $\Delta\nu$ values ($\Delta\nu = \nu_{asym} - \nu_{sym}$) are smaller than 200 cm^{-1} consistent with a bridging coordination mode of the carboxylate groups.[26] The spectrum of the Fe^{III} dimer shows a weak broad band at ca. 3435 cm^{-1}, attributed to the Fe^{III}-bridging hydroxido groups.

Mass Spectrometry

Mass spectrometric data of the three complexes were obtained in acetonitrile and show the distinct isotopic patterns of the corresponding metal ion combinations (Figures 6, 7, and 8). The spectrum of the $Fe^{III}Zn^{II}$ complex shows a mass peak at m/z = 715.1523 with a peak separation of 1 unit, indicating a singly charged species corresponding to $[Fe^{III}Zn^{II}(BMMHP)(CH_3COO)_2]^+$ (calcd. 715.1530) (Figure 6). The results for the Fe^{III} dimer $[Fe_2(BMMHPH)_2(\mu\text{-}OH)_2](BPh_4)_2$ (Figure 7) show a mass peak at m/z = 533.1977. The mass peak separation is again 1 unit, indicating disassociation of the dimer in solution to yield only the monomeric unit $[Fe^{III}(BMMHP)]^+$ (calcd. 533.1972).

Recording the mass spectrum of the $Fe^{III}{}_2Mg^{II}$ trimer immediately after dissolution in ice-cold acetonitrile (ca. 0 °C) resulted in three major mass peaks at m/z = 636.1, 647.1 and 705.1, and two very small mass peaks at m/z = 661.1 and 675.1 [Figure 8(a)]. The isotopic pattern at m/z = 636.1 is separated by 0.5 units and was assigned to the doubly charged species $[Fe_2Mg(BMMHPH)_2(CH_3COO)_2(CH_3O)_2]^{2+}$ (calcd. 636.299) corresponding to the $Fe^{III}{}_2Mg^{II}$ trimer, in agreement with the crystal structure. The remaining four mass peaks at m/z = 647.1, 661.1, 675.1 and 705.1 exhibit peak separations of 1 unit and correspond to $[Fe^{III}Mg^{II}(BMMHP)(CH_3O)(CH_3COO)]^+$ (calcd. 647.214), $[Fe^{III}Mg^{II}(BMMHP)(CH_3O)(OH)_2K]^+$ (calcd. 661.206), $[Fe^{III}Mg^{II}(BMMHP)(CH_3COO)_2]^+$ (calcd. 675.209) and

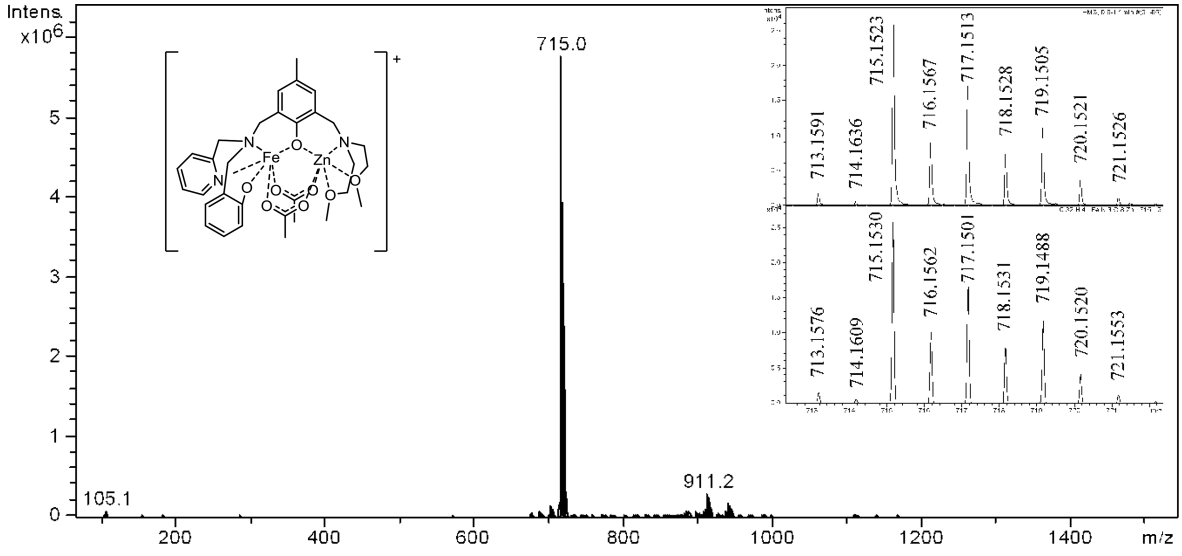

Figure 6. Low-resolution mass spectrometric data of $[Fe^{III}Zn^{II}(BMMHP)(CH_3COO)_2](BPh_4)$ in acetonitrile. Inset shows high-resolution positive ESI and calculated isotopic pattern.

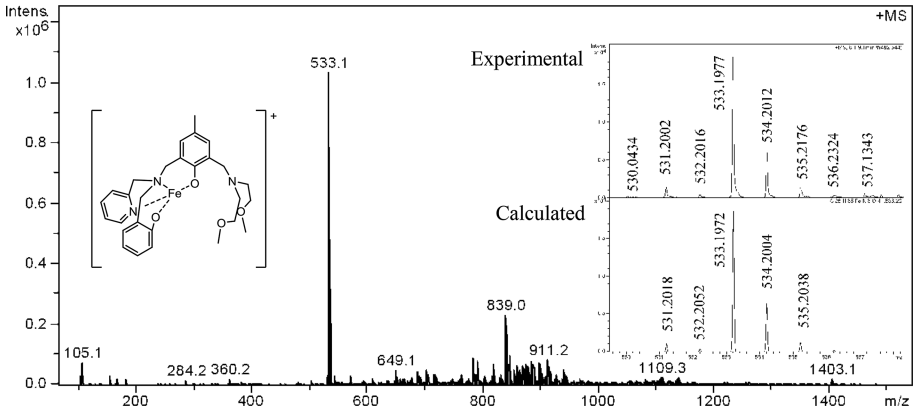

Figure 7. Low-resolution mass spectrometric data of $[Fe^{III}_2(BMMHPH)_2(\mu\text{-}OH)_2](BPh_4)_2$ in acetonitrile. Inset shows high-resolution positive ESI and calculated isotopic pattern of the monomer unit $[Fe(BMMHP)]^+$.

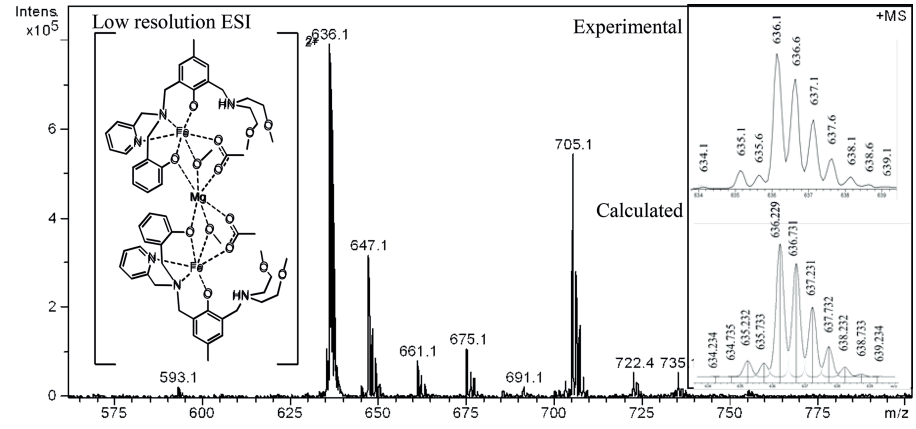

(a)

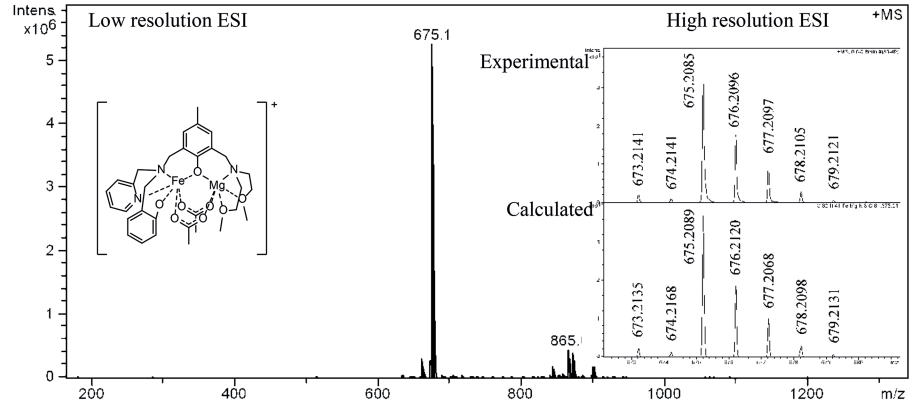

(b)

Figure 8. (a) Low-resolution mass spectrometric data of $[Fe^{III}_2Mg^{II}(BMMHPH)_2(CH_3COO)_2(CH_3O)_2](BPh_4)_2$ prepared in cold acetonitrile. Inset shows the experimental and calculated isotopic pattern of the doubly charged mass peak at m/z = 636.1. (b) Low-resolution mass spectrometric data of $[Fe^{III}_2Mg^{II}(BMMHPH)_2(CH_3COO)_2(CH_3O)_2](BPh_4)_2$ after 90 min in acetonitrile. Inset shows high-resolution positive ESI and calculated isotopic pattern.

$[Fe^{III}Mg^{II}(BMMHP)(CH_3COO)(CH_3O)(OH)(H_2O)Na]^+$ (calcd. 705.217), respectively. Recording the mass spectrum of the same sample after 90 min resulted only in m/z = 675.1 [high resolution: 675.2085; Figure 8(b)], assigned to the species $[Fe^{III}Mg^{II}(BMMHP)(CH_3COO)_2]^+$ (calcd. 675.2089).

Magnetic Studies for $[Fe^{III}_2(BMMHPH)_2(\mu\text{-}OH)_2](BPh_4)_2$

Solid-state magnetic susceptibility of $[Fe^{III}_2(BMMHPH)_2(\mu\text{-}OH)_2](BPh_4)_2$ was measured over the temperature range from 300 to 2 K. The magnitude and temperature dependence of the magnetic susceptibility are typical of an $S_1 = S_2 = 5/2$ dimer,[27] with $\chi_M T$ decreasing steadily from 8.04 $cm^3 mol^{-1} K$ at 300 K (calcd. 8.76 $cm^3 mol^{-1} K$) to 5.79 $cm^3 mol^{-1} K$ at 45 K, followed by a rapid decrease to near zero at 2 K (0.34 $cm^3 mol^{-1} K$). The data were fit to an equation based on a spin interaction Hamiltonian $\hat{H} = -2J\hat{S}_1 \cdot \hat{S}_2$ ($S_1 = S_2 = 5/2$).[28] The equation included a factor ρ accounting for the percentage of monomer impurity. A non-linear least-squares fit ($g = 2$) gave $J = -1.76 \pm 0.03$ cm^{-1}, and $\rho = 0.07 \pm 0.01$. The susceptibility data and the theoretical fit are shown in Figure 9. The J value of –1.76 cm^{-1} is below the range observed for similar Fe^{III}–(μ-OH)$_2$–Fe^{III} diamond core complexes (J = –6.0 to –13.0 cm^{-1})[24,25,29] and indicates very weak antiferromagnetic interactions between the two d^5 centres. The markedly weaker interactions in this complex may be due in part to longer Fe–O bonds (on average ca. 0.036 Å longer) and smaller Fe–O–Fe angles (by ca. 3.4°).[30]

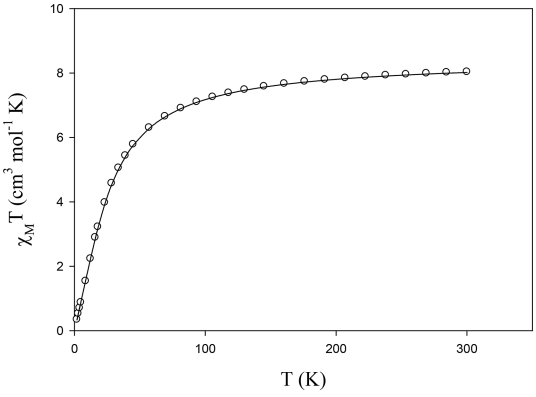

Figure 9. Temperature dependence of the molar paramagnetic susceptibility of $[Fe^{III}_2(BMMHPH)_2(\mu\text{-}OH)_2](BPh_4)_2$ (circles). The solid line represents the nonlinear least-squares fit of the data (g = 2; $J = -1.76 \pm 0.03$ cm^{-1}; $\rho = 0.07 \pm 0.01$) to an equation based on a spin interaction Hamiltonian $\hat{H} = -2J\hat{S}_1 \cdot \hat{S}_2$ ($S_1 = S_2 = 5/2$).[28] The equation included a factor ρ accounting for the percentage of monomer impurity.

Kinetic Studies

Phosphatase-like activities of $[Fe^{III}Zn^{II}(BMMHP)(CH_3COO)_2](BPh_4)$ and $[Fe^{III}_2(BMMHPH)_2(\mu\text{-}OH)_2](BPh_4)_2$ were measured by using the activated substrate BDNPP, and the dependence of catalysis on the pH was determined in the range between pH = 5 and 10.5 [Figure 10(a)]. The pH rate profiles for the two complexes are different with the FeZn complex exhibiting a limiting rate at pH > 9, whereas the profile for the Fe dimer appears to follow a typical bell-shaped curve. For the latter the pH profile was fitted [Figure 10(a)] by using the Equation (1):[31]

$$v_0 = \frac{v_{max}}{\left(1 + \frac{[H^+]}{K_{a1}} + \frac{K_{a2}}{[H^+]}\right)} \quad (1)$$

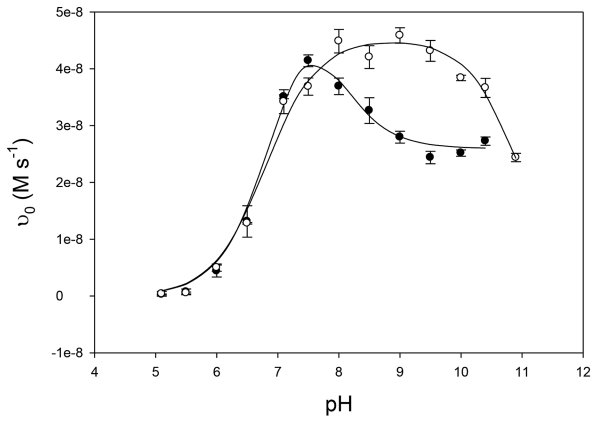

(a)

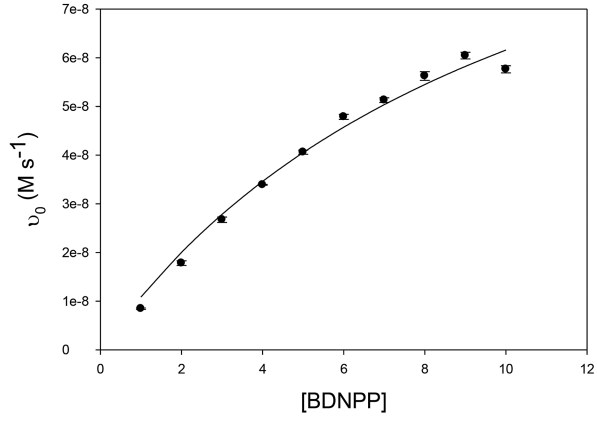

(b)

Figure 10. (a) Plot of the pH dependence of the initial rate of BDNPP hydrolysis (5 mM) by $[Fe^{III}Zn^{II}(BMMHP)(CH_3COO)_2](BPh_4)$ (filled circles) and $[Fe^{III}_2(BMMHPH)_2(\mu\text{-}OH)_2](BPh_4)_2$ (empty circles): for the FeZn complex the fit to the data using Equation (2) is shown as solid line {the kinetic pK_a values for $[Fe^{III}Zn^{II}(BMMHP)(CH_3COO)_2](BPh_4)$ were found to be 6.89, 7.37 and 9.00 with $\alpha = 3.0$ and $\beta = 0.61$}; for the Fe dimer the fit to the data employed Equation (2), the kinetic pK_a values were found to be 6.80 and 10.9. (b) Plot of the substrate dependence of the initial rate of BDNPP hydrolysis (5 mM) by $[Fe^{III}Zn^{II}(BMMHP)(CH_3COO)_2](BPh_4)$ (filled circles); the fit to the data using the Michaelis–Menten equation is shown as solid line (pH = 7.5; $k_{cat} = 3.20 \pm 0.38 \times 10^{-3}$ s^{-1} and $K_M = 10.8 \pm 2.1$).

In this equation, v_0 is the reaction rate of formation of DNP (M s^{-1}) and v_{max} is the maximum reaction rate. The two K_a values are the acid dissociation constants for two catalytically relevant protonated moieties; the corresponding pK_a values were found to be 6.80 and 10.9. For $[Fe^{III}Zn^{II}(BMMHP)(CH_3COO)_2](BPh_4)$ the data were fit to a model, which assumes three deprotonation equilibria and competitive reaction pathways, described by the terms α and β in Equation (2):[12i,23b,31]

$$\nu_0 = \frac{\nu_{max}\left(1+\frac{\alpha K_{a2}}{[H^+]}+\frac{\beta K_{a3}}{[H^+]}\right)}{\left(1+\frac{[H^+]}{K_{a1}}+\frac{K_{a2}}{[H^+]}\right)} \quad (2)$$

The factors α and β (= 3.0 and 0.6, respectively) relate the activity of the species at high pH to the maximum activity.[31] Based on this model the kinetic pK_a values for $[Fe^{III}Zn^{II}(BMMHP)(CH_3COO)_2](BPh_4)$ were estimated to be 6.89, 7.37 and 9.00 [Figure 10(a)] and are in relatively good agreement with the separately determined spectrophotometric values of 6.11, 7.30 and 10.1.

The substrate concentration dependence of catalysis for $[Fe^{III}Zn^{II}(BMMHP)(CH_3COO)_2](BPh_4)$ was also measured at pH = 7.5; Michaelis–Menten-type behaviour was observed, and the data were fitted by using non-linear least-squares analysis to provide an estimate for V_{max} = $1.28 \pm 0.15 \times 10^{-7}$ M s^{-1}, with k_{cat} (V_{max}/[complex]) = $3.20 \pm 0.38 \times 10^{-3}$ s^{-1} and K_M = 10.8 ± 2.1 mM [Figure 10(b)]. The rate of hydrolysis of BDNPP (5 mM; pH = 7.5) was linear for complex concentrations from 20 to 160 μM. The kinetic parameter k_{cat} shows an acceleration of the reaction rate ca. 10^4-fold over the uncatalyzed hydrolysis of BDNPP ($k_{uncat} = 1.87 \times 10^{-7}$ s^{-1}).[32]

Previously, the pH dependence of similar FeZn complexes for the hydrolysis of substrates such as BDNPP has been described by three equilibria (L = $BMMHP^{2-}$)[12d,12i,23b] by assuming that the μ-CH_3COO^- groups are replaced by at least one or more aqua ligands to form the catalytically competent species:

$[(OH_2)Fe^{III}(OH_2)(L)Zn^{II}(OH_2)]/[(OH)Fe^{III}(OH_2)(L)Zn^{II}(OH_2)]$ pK_{a1}

$[(OH)Fe^{III}(OH_2)(L)Zn^{II}(OH_2)]/[(OH)Fe^{III}(\mu\text{-}OH)(L)Zn^{II}(OH_2)]$ pK_{a2}

$[(OH)Fe^{III}(\mu\text{-}OH)(L)Zn^{II}(OH_2)]/[(OH)Fe^{III}(\mu\text{-}OH)(L)Zn^{II}(OH)]$ pK_{a3}

The three pK_a values are typically of the order p$K_{a1} \approx 5$, p$K_{a2} \approx 6$–7 and p$K_{a3} \approx 8$–9.[12d,12i,23b] As shown above, three kinetically relevant pK_a values are also observed for the FeZn complex in this study (6.89, 7.37 and 9.00).[12i,23b] As both the FeZn and Fe dimer complexes exhibit a pK_a of ca. 6.9 this has been assigned to the deprotonation of the Fe^{III}-OH_2 moiety; for the FeZn complex the second pK_a is assigned to the deprotonation of the bridging Fe–(OH_2)–Zn species and the third to the deprotonation of the terminal Zn–OH_2 group. This assignment assumes that the μ-OH group forms after the deprotonation of what is originally a terminal water ligand, presumably bound to the Fe^{III} atom.[33]

The proposed catalytic mechanism of the native enzyme is thought to involve the binding of the substrate to the divalent centre, facilitated by the histidine residues, and is followed by nucleophilic attack upon the phosphorus atom by a terminally Fe^{III}-bound hydroxido group.[10] The proposal is that coordination of the substrate to the Zn^{II} site causes polarization of the O–P bond, activating the phosphorus atom for nucleophilic attack, and strong Lewis acidity of Fe^{III} promotes the formation of the nucleophilic hydroxido group at low pH, allowing catalysis to occur under acidic conditions.[10] In the case of $Fe^{III}Zn^{II}$ mimics of the PAP enzyme, monodentate binding of the substrate is proposed where the substrate exchanges with a Zn^{II}-coordinated water molecule, and nucleophilic attack by an Fe^{III}-bound hydroxido group upon the phosphorus atom is followed by release of the products.[10,11,12d] Overlaying a speciation plot of the active FeZn complexes in solution, determined from the respective pK_a values, with the pH rate profile (Figure 11) suggests that in the pH range of ca. 5–10.5 two active species of the complex are present, $[(OH)Fe^{III}(OH_2)(L)Zn^{II}(OH_2)]$ at the lower pH end and $[(OH)Fe^{III}(\mu\text{-}OH)(L)Zn^{II}(OH_2)]$ (L = BMMHP) at the other extreme; the latter is the more effective catalyst (α = 3; β = 0.6). The assignment of the origins of pK_{a1} and pK_{a2} is problematic. On one hand assigning pK_{a2} to the deprotonation of a bridging water molecule and pK_{a1} to deprotonation of the water molecule terminally bound to Fe^{III} would imply that the latter is more acidic than the water molecule bridging the Fe^{III} and Zn^{II} atoms – in other words, the terminal water molecule deprotonates more easily than the bridging one. The pK_{a1} of 6.7 is reasonable for a terminally Fe^{III}-bound water molecule. If the assignment is made such that pK_{a1} describes the deprotonation of the bridging water molecule then pK_{a2} is assigned to the deprotonation of Fe–OH_2, the terminal water molecule. However, the fact that both the $Fe^{III}Zn^{II}$ and Fe^{III}_2 complexes display a pK_a of ca. 6.9 would imply that this deprotonation is associated with the Fe^{III} component. It might be that the second deprotonation occurs at a second Fe^{III}-bound water molecule, and upon deprotonation that terminal water molecule becomes bridging, i.e. Fe–OH–Zn. In either case the active species remain species $[(OH)Fe^{III}(\mu\text{-}OH_2)(L)Zn^{II}(OH_2)]$ and $[(OH)Fe^{III}(\mu\text{-}OH)(L)Zn^{II}(OH_2)]$ (Figure 11) with some activity arising from $[(OH_2)Fe^{III}(\mu\text{-}OH_2)(L)Zn^{II}(OH_2)]$. This observation may indicate that the hydrolysis-initiating nucleophile changes from a terminally, Fe^{III}-coordinated hy-

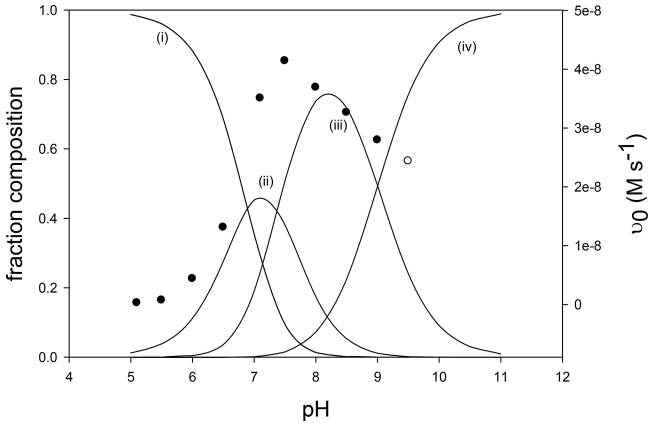

Figure 11. Species distribution curve as a function of pH. The solid lines represent the complexes (i) $[(OH_2)Fe^{III}(OH_2)(L)Zn^{II}(OH_2)]$, (ii) $[(OH)Fe^{III}(OH_2)(L)Zn^{II}(OH_2)]$, (iii) $[(OH)Fe^{III}(\mu\text{-}OH)(L)Zn^{II}(OH_2)]$ and (iv) $[(OH)Fe^{III}(\mu\text{-}OH)(L)Zn^{II}(OH)]$ (L = $BMMHP^{2-}$); the filled circles represent the pH-initial rate profile of the complex with ν_0 [M s^{-1}] shown on the right-hand axis.

droxido group to a metal ion-bridging hydroxide ion as the pH is increased. The presence of two possible nucleophiles is in agreement with mechanistic models proposed for PAP, where the processive cleavage of the two ester bonds of diphosphate substrates was associated with the sequential actions of a hydroxide ion located in the second coordination sphere of the Fe^{III} atom and a hydroxide ion bridging the two metal ions in the active site.[34] Furthermore, studies with a distantly related organophosphate-degrading enzyme (OpdA) also demonstrated that a change in pH can induce a change in the identity of the relevant nucleophile of the reaction.[35] Thus, the FeZn biomimetic described here is not only capable of modelling structural aspects and catalytic properties of corresponding enzyme systems, but it is also able to imitate mechanistic flexibility.

At high pH deprotonation of the terminally Zn^{II}-bound H_2O to form a less labile Zn^{II}–OH bond decreases substrate binding and, hence, catalytic activity.[12c,12i] The presence of a limiting rate at high pH has been observed in other models and is suggestive of a second kinetic pathway.[12c,12d,12i,12p,12q,23b,36] The proposed reaction scheme is shown in Figure 12. The shape of the pH rate profile indicates that sufficient coordination flexibility of the deprotonated species permits substrate coordination despite the presence of a less labile Zn–OH bond.[23b]

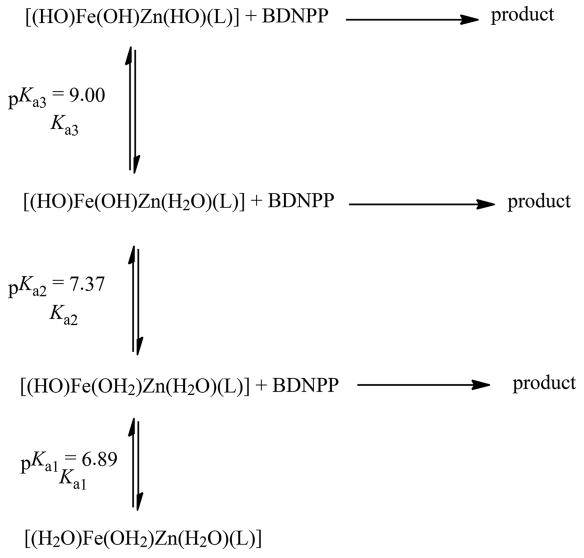

Figure 12. Proposed diprotic equilibrium scheme for two different active species (L = $BMMHP^{2-}$) at high and low pH [BDNPP = bis(2,4-dinitrophenyl) phosphate].[23b,31]

The data in Table 1 summarize many of the heterodimetallic systems reported as mimics for the PAP metalloenzymes. A variety of divalent metal ions have been incorporated into these ligands, many with true biological relevance, others (for example Hg^{II}, Cd^{II}) less relevant. What is clear from the extensive data is that these systems consistently exhibit k_{cat} values of the order of 10^{-4} to 10^{-3} s^{-1}, with a more expansive range of K_M values (2–90 mM), considerably less efficient than the enzyme itself, albeit the latter with biologically more relevant substrates (p-NPP. ATP, ADP).[37] The identity of the divalent ion appears to have little effect on k_{cat}. In the present case the complex [Fe^{III}-Zn^{II}(BMMHP)$(CH_3COO)_2$](BPh_4) appears to be a suitable model for PAP, exhibiting catalytic activity similar to other related model complexes in addition to characterized regioselectivity in metal ion coordination (Figure 1 and Table 1).[12i,12n,12p,12q,19]

Table 1. Catalytic parameters of a selection of model complexes.

Ligand	Metal centre	k_{cat} [s^{-1}]	K_M [mM]	pH
H_2BPBPMP (a)	$Fe^{III}Zn^{II}$[12d]	7.31×10^{-4}	8.10	6.1
(a)	$Fe^{III}Zn^{II}$[12c]	9.13×10^{-4}	4.20	6.5
(a)	$Fe^{III}Mn^{II}$[12m]	4.51×10^{-4}	2.10	6.7
(a)	$Fe^{III}Ni^{II}$[12o]	4.47×10^{-4}	3.85	6.0
(a)	$Fe^{III}Cu^{II}$[12n]	1.77×10^{-3}	11	6.8
(a)	$Fe^{III}Cd^{II}$[12q]	1.08×10^{-3}	1.75	6.5
(a)	$Fe^{III}Hg^{II}$[12q][a]	4.42×10^{-4}	7.29	6.5
(a)	$Fe^{III}Co^{II}$[12p]	1.42×10^{-3}	92.7	7.0
(a)	$Ga^{III}Co^{II}$[12p]	1.87×10^{-3}	88.1	7.0
(e)	$Fe^{III}Zn^{II}$[43]	6.76×10^{-4}	27.8	6.5
(e)	$Fe^{III}Co^{II}$[43]	3.14×10^{-4}	9.80	6.5
(e)	$Fe^{III}Ni^{II}$[43]	1.92×10^{-4}	9.40	6.5
(e)	$Fe^{III}Mn^{II}$[43]	4.00×10^{-4}	14.6	6.5
(f)	$Fe^{III}Mn^{II}$[42]	–	3.84	9.0
(h)	$Fe^{III}Zn^{II}$[12i]	3.8×10^{-3}	4.1	6.5
(j)	$Fe^{III}Cu^{II}$[19]	1.88×10^{-3}	3.08	7
(j)	$Fe^{III}Zn^{II}$[12b]	9.02×10^{-4}	3.55	7.0
(k)	$Fe^{III}Fe^{II}$[11a]	1.33×10^{-3}	1.94	6
(l)	$Fe^{III}Fe^{II}$	1.14×10^{-3}	2.30	
BMMHP	$Fe^{III}Zn^{II}$[b]	3.2×10^{-3}	10.8	7.5

[a] Complex found to be a dimer of dimers. [b] This work.

Conclusions

The ligand $BMMHPH_2$ offers the potential for site-specific binding of Fe^{III} and Zn^{II} resulting in the complex [$Fe^{III}Zn^{II}$(BMMHP)$(CH_3COO)_2$](BPh_4). The catalytic activity of this complex towards the hydrolysis of the activated phosphate ester BDNPP is comparable to that displayed by similar model systems.[12d,12i,23b] Enhancement of this type of model system with second coordination sphere may offer the opportunity for enhanced activity and a more defined structural model for the plant PAP metalloenzyme.[11a–11c,36]

Experimental Section

General Methods: ^1H and ^{13}C NMR spectra were recorded with a 300, 400 or 500 MHz Bruker Avance spectrometer. Data were processed with TOPSPIN from Bruker. Chemical shifts of the final ligand were assigned by using two-dimensional correlation spectroscopy (COSY), heterodinuclear single quantum correlation (HSQC), heterodinuclear multiple bond connectivity (HMBC) and distortionless enhancement by polarization transfer (DEPT). Positive ion electrospray mass spectrometry was carried out by using a Q-Star time-of-flight mass spectrometer, data processed with Bruker Compass Data Analysis 4.0 software. Measurements of organic compounds were carried out in methanol, and of complexes in acetonitrile. Calculated isotopic patterns for both high- and low-resolution spectra were obtained by using Bruker built-in isotope pattern predictors. IR spectra were recorded by using a Perkin-

Elmer FT-IR/NIR Frontier spectrometer with a diamond/ZnSe crystal by using a Universal ATR sampling accessory. Elemental analysis for carbon, hydrogen and nitrogen was carried out at the University of Queensland by Mr. George Blazak or Dr. Michael Nefedov. Carbon, hydrogen, nitrogen, iron, zinc and magnesium elemental analyses were carried out at the Campbell Laboratories of the University of Otago.

X-ray Crystallography: Crystallographic measurements were carried out by using an Oxford Diffraction Gemini Ultra dual-source (Mo-K_α, λ = 0.71073 Å and Cu-K_α, λ = 1.5418 Å) CCD diffractometer. Crystal structures were solved by either direct methods (SIR-92) or Patterson's method (SHELX 86) and refined (SHELXL 97) by full-matrix least-squares methods.[38] These programs were accessed through the WINGX 1.70.01 crystallographic collective package.[39] All non-hydrogen atoms were refined anisotropically unless they were disordered. Hydrogen atoms were fixed geometrically and were not refined. CCDC-1057035 {for $[Fe^{III}Zn^{II}(BMMHP)(CH_3COO)_2](BPh_4)$}, -1057036 {for $[Fe^{III}_2(BMMHPH)_2(\mu\text{-}OH)_2](BPh_4)_2$}, and -1057037 {for $[Fe^{III}_2Mg^{II}(BMMHPH)_2(CH_3COO)_2(CH_3O)_2](BPh_4)_2$} contain the supplementary crystallographic data for this paper. These data can be obtained free of charge from The Cambridge Crystallographic Data Centre via www.ccdc.cam.ac.uk/data_request/cif.

Magnetic Susceptibility Measurements: Solid-state magnetic susceptibility data were collected by using an MPMS-XL 5T superconducting quantum interference device (SQUID) from Quantum Design at Monash University, Victoria, by Dr. Boujemaa Moubaraki. Measurements were collected over the temperature range 300–2 K (zero-field cooled method).

Phosphatase Studies: Kinetic studies of the phosphatase-like activity towards the highly activated substrate bis(2,4-dinitrophenyl) phosphate (BDNPP) were carried out by monitoring the formation of 2,4-dinitrophenol (DNP) at 400 nm. A Varian Cary50 Bio UV/Vis spectrophotometer was employed with 10 mm quartz cuvettes and a Peltier temperature controller to maintain a temperature of 298 K. Measurements were taken by using a 50:50 buffer/acetonitrile solution, 40 μM complex and 5 mM BDNPP in acetonitrile. The aqueous buffer consisted of 50 mM MES [2-(morpholino)ethanesulfonic acid] (pH = 5.50–6.70), HEPES [4-(2-hydroxyethyl)-1-piperazineethanesulfonic acid] (pH = 7.00–8.50), CHES [2-(cyclohexylamino)ethanesulfonic acid] (pH = 9.00–10.00) and CAPS [3-(cyclohexylamino)propanesulfonic acid] (pH = 10.5–11) at constant ionic strength by using 250 mM $LiClO_4$. The pH was adjusted by using NaOH to give buffers ranging from pH = 5.0 to 10.5. These were then treated with Chelex for 24 h and filtered through a 0.45 μm Millex syringe-driven filter. The pH values reported refer to the aqueous component; it should be noted, however, that the pH of a solution of buffer was the same within error as a 1:1 mixture of buffer and acetonitrile.[40] Measurements were carried out as follows: complex and buffer were mixed and left for 1 min before the addition of the substrate. Once the substrate had been added, the reaction was allowed 15 s in the measurement chamber for the temperature to stabilise and the reaction to equilibrate. The initial rates were determined over a period of 3 min, and all measurements were carried out in triplicate. The pH dependence of hydrolysis was measured over the range of pH = 5.0 to 10.5.[31] Substrate and complex concentration dependence at optimum pH were also measured, and the substrate dependence data were fit to the Michaelis–Menten equation.[31]

UV/Vis Titration: Thermodynamic pK_a values were determined by using UV/Vis spectrophotometry. Measurements of individually prepared samples were carried out in 50:50 acetonitrile/buffer solutions by using 40 μM complex and pH values ranging from 4.6 to 10.5 at 25 °C. Each measurement was carried out by the initial mixing of buffer (500 μL) and acetonitrile (400 μL) in a cuvette, followed by the addition of the complex (100 μL, 400 μM), after which the cuvette was allowed to remain in the measurement chamber for 1 min before the measurement was taken (200–800 nm). Data were fitted to three equilibrium constants by using the program ReactLab EQUILIBRIA.[41]

Ligand Synthesis: The organic compounds (2-hydroxybenzyl)(2-pyridylmethyl)amine[17] (HBPA) and 2,6-bis(chloromethyl)-4-methylphenol[18] were synthesised according to previously published procedures. BDNPP was synthesised with slight modifications according to a previously published procedure.[32]

2-{[Bis(2-methoxyethyl)amino]methyl}-6-{[(2-hydroxybenzyl)(2-pyridylmethyl)amino]methyl}-4-methylphenol ($BMMHPH_2$): A solution of HBPA (0.99 g, 4.6 mmol), bis(2-methoxyethyl)amine (0.61 g, 4.6 mmol) and triethylamine (0.91 g, 9.0 mmol) in THF (4.5 mL) was cooled to 0 °C. After the dropwise addition of 2,6-bis(chloromethyl)-4-methylphenol (1.1 g, 5.4 mmol) in THF (4 mL), the mixture was stirred at room temperature for 24 h. The mixture was filtered to remove triethylamine hydrochloride, and the solvent was removed in vacuo to yield a yellow oil (2.51 g). The desired product was isolated as a yellow oil by flash column chromatography [silica gel 100 g, h = 20 cm, *i.d.* = 5 cm, loaded with 1:1 chloroform/petroleum ether, eluted with 1:1 ethyl acetate/petroleum ether (2000 mL) and neat ethyl acetate (300 mL), R_f = 0.38 (1:8 methanol/petroleum ether), 0.36 g, 16%]. ^{1}H NMR ($CDCl_3$, 500.13 MHz): δ = 8.56 (d, 1 H, J = 4.4 Hz, H^{20}), 7.64 (td, 1 H, J = 1.8, 7.7 Hz, H^{18}), 7.42 (d, 1 H, J = 7.7 Hz, H^{17}), 7.16 (t, 1 H, H^{19}), 7.12 (td, 1 H, J = 1.5, 7.7 Hz, H^{23}), 7.02 (dd, 1 H, J = 1.5, 7.4 Hz, H^{21}), 6.94 (d, 1 H, J = 1.9 Hz, H^1), 6.81 (dd, 1 H, J = 1.0, 8.1 Hz, H^{24}), 6.74 (td, H, J = 1.2, 7.4 Hz, H^{22}), 6.71 (s, 1 H, H^5) 3.84 (s, 2 H, H^{11}), 3.80 (s, 4 H, $H^{8,10}$), 3.71 (s, 2 H, H^9), 3.53 (t, 4 H, $H^{16,27}$), 3.31 (s, 6 H, $H^{26,28}$), 2.80 (t, 4 H, $H^{12,13}$), 2.20 (s 3 H, H^7) ppm. ^{13}C NMR ($CDCl_3$, 75.47 MHz): δ = 158.0 (C^{14}), 157.6 (C^{25}), 154.2 (C^3), 148.7 (C^{20}), 136.6 (C^{18}), 131.1 (C^1), 129.3 (C^{21}), 128.9 (C^5), 128.6 (C^{23}), 127.7 (C^6), 123.4 (C^{17}), 123.2 (2C, $C^{2,4}$), 122.6 (C^{15}), 122.1 (C^{19}), 118.9 (C^{22}), 116.1 (C^{24}), 70.1 ($C^{16,27}$), 59.3 (C^{11}), 58.7 (2C, $C^{26,28}$), 56.9 ($C^{8,10}$), 53.2 (2C, $C^{12,13}$), 52.9 (C^9), 20.4 (C^7) ppm. FT-IR: $\tilde{\nu}$ = 3100–2600 (m, aryl C–H str, O–H, OC–H^3), 1588 (s, aryl C=C str), 1480 (s, C–H^2 deform), 1362 (m, sym deform C–H^3), 1251 (s, C–O–C), 1112 (s, aryl CO–H), 972 (m), 862 (m), 751 (s, deform vib, 4 neighbouring arom C–H) cm^{-1}. ESI MS (CH_3CN): m/z = 480.1 $[C_{28}H_{38}N_3O_4]^+$.

Synthesis of Metal Complexes

$[Fe^{III}Zn^{II}(BMMHP)(CH_3COO)_2](BPh_4)$: Iron(II) acetate (31 mg, 0.18 mmol) in methanol (10 mL) was added dropwise to a solution of $BMMHPH_2$ (86 mg, 0.18 mmol) in methanol (10 mL), and the mixture was stirred for 10 min. Zinc(II) acetate (33 mg, 0.18 mmol) in methanol (10 mL) was added and the mixture heated to reflux for 30 min. The solution was cooled, and a solution of sodium tetraphenylborate (120 mg, 0.36 mmol) in methanol (10 mL) was added. After filtering, the solution was allowed to stand in an open conical flask at room temperature. Dark purple needle-shaped crystals of diffraction quality formed after 7 d (43 mg, 23%). ESI MS (CH_3CN): m/z = 715.1523 $[C_{32}H_{41}FeN_3O_8Zn]^+$. $C_{56}H_{61}BFeN_3O_8Zn$ (1036.1): calcd. C 64.91, H 5.93, Fe 5.39, N 4.06, Zn 6.31; found C 65.21, H 6.03, Fe 5.05, N 4.13, Zn 6.15. UV/Vis (CH_3CN): λ_1 = 275 nm (14000 L mol^{-1} cm^{-1}), λ_2 = 335 nm (3900 L mol^{-1} cm^{-1}), λ_3 = 553 nm (3500 L mol^{-1} cm^{-1}). FT-IR: $\tilde{\nu}$ = 3070–2830 (w, aryl C–H str, OC–H^3), 1589 (s, antisym str, acetate), 1478 (s, C–H^2 deform), 1424 (s, sym str, acetate), 1295 (s, C–O–C),

1264 (s, C–O–C), 1094 (m, aryl C–O) 1023 (m), 733 (s, deform vib, 4 neighbouring arom C–H), 703 (s, deform vib, 4 neighbouring arom C–H), 611 (s) cm^{-1}.

$[Fe^{III}_2(BMMHPH)(\mu\text{-}OH)_2](BPh_4)_2$: A solution of iron(II) acetate (31 mg, 0.18 mmol) and $BMMHPH_2$ (85 mg, 0.18 mmol) in methanol (40 mL) was stirred for 10 min. A solution of sodium tetraphenylborate (120 mg, 0.35 mmol) was added to the mixture, which was then filtered and allowed to concentrate to dryness. The purple solid was redissolved in acetonitrile, and diffusion of the solution over water resulted in the formation of dark red diamond-shaped crystals of diffraction quality (52 mg, 33%). ESI MS (CH_3CN): *m/z* = 533.1977 $[C_{28}H_{35}FeN_3O_4]^+$. $C_{104}H_{114}B_2Fe_2N_6O_{10}$ (1741.4): calcd. C 71.73, H 6.60, N 4.83; found C 71.37, H 6.67, N 4.85. UV/Vis (CH_3CN): λ_1 = 203 nm (93000 $L\,mol^{-1}\,cm^{-1}$), λ_2 = 493 nm (3000 $L\,mol^{-1}\,cm^{-1}$). FT-IR: $\tilde{\nu}$ = 3435 (w, br., μ-O–H), 3054–2830 (w, aryl C–H str, OC–H^3), 1596 (m, aryl C=C str), 1475 (s, C–H^2 deform), 1269 (s, C–O–C), 1087 (m, aryl C–O), 1033 (m), 881 (m), 846 (m), 733 (s, deform vib, 4 neighbouring arom C–H), 705 (s, deform vib, 4 neighbouring arom C–H), 610 (s) cm^{-1}. μ_{eff} (solid; 300 K) = 8.02 μ_B.

$[Fe^{III}_2Mg^{II}(BMMHPH)_2(CH_3COO)_2(CH_3O)_2](BPh_4)_2$: Iron(II) acetate (33mg, 0.19 mmol) in methanol (5 mL) was added dropwise to a solution of $BMMHPH_2$ (90 mg, 0.19 mmol) in methanol (8 mL) and the mixture stirred for 10 min. Magnesium(II) acetate hydrate (40 mg, 0.19 mmol) in methanol (6 mL) was added and the mixture heated to reflux for 30 min. Once cool, a solution of sodium tetraphenylborate (130 mg, 0.38 mmol) in methanol (4 mL) was added. After filtering, the mixture was allowed to stand in an open conical flask at room temperature. The solid that formed was collected, redissolved in hot methanol (50 mL) and allowed to stand in a covered conical flask. Orange crystals of diffraction quality formed after 7 d (26 mg, 14%). ESI MS (CH_3CN): *m/z* = 636.1 $[C_{62}H_{84}Fe_2MgN_6O_{14}]^{2+}$ 647.1 $[C_{31}H_{41}FeMgN_3O_7]^+$, 661.1 $[C_{29}H_{40}FeKMgN_3O_7]^+$, 705.1 $[C_{31}H_{44}FeMgN_3NaO_9]^+$, 675.2085 $[C_{32}H_{41}FeMgN_3O_8]^+$. $C_{56}H_{61}BFeMgN_3O_8$ (995.1): calcd. C 69.11, H 6.54, Fe 5.84, Mg 1.27, N 4.40; found C 69.0, H 6.59, Fe 5.65, Mg 1.34, N 4.44. UV/Vis (CH_3CN): λ_1 = 210 nm (47000 $L\,mol^{-1}\,cm^{-1}$), λ_2 = 465 nm (2340 $L\,mol^{-1}\,cm^{-1}$). FT-IR: $\tilde{\nu}$ = 3057–2812 (m, aryl C–H str, OC–H^3), 1598 (s, antisym str, acetate), 1477 (s, C–H^2 deform), 1399 (s, sym str, acetate), 1274 (s, C–O–C), 1120 (m, aryl C–O), 1073 (m, aryl C–O), 953 (m), 882 (m), 732 (s, deform vib, 4 neighbouring arom C–H), 705 (s, deform vib, 4 neighbouring arom C–H), 611 (s) cm^{-1}.

Acknowledgments

The receipt of an ARC Discovery Grant (DP150104358) is acknowledged. In addition, G. S. also acknowledges the receipt of an ARC Future Fellowship (FT120100694).

[1] T. T. Chen, F. W. Bazer, J. J. Cetorelli, W. E. Pollard, R. M. Roberts, *J. Biol. Chem.* **1973**, *248*, 8560–8566.
[2] H. D. Campbell, B. Zerner, *Biochem. Biophys. Res. Commun.* **1973**, *54*, 1498–1503.
[3] J. L. Beck, L. A. McConachie, A. C. Summors, W. N. Arnold, J. De Jersey, B. Zerner, *Biochim. Biophys. Acta Protein Struct. Mol. Enzymol.* **1986**, *869*, 61–68.
[4] G. G. Bozzo, W. C. Plaxton, "Tomatoes and Tomato Products", in *Nutritional, Medicinal and Therapeutic Properties* (Eds.: Victor R. Preedy, Ronald R. Watson), Science Publishers, Inc. **2008**, pp. 215–234.
[5] S. K. Hefler, B. A. Averill, *Biochem. Biophys. Res. Commun.* **1987**, *146*, 1173–1177.
[6] B. R. LeBansky, T. D. McKnight, L. R. Griffing, *Plant Physiol.* **1992**, *99*, 391–395.
[7] Q. Zhang, C. Wang, J. Tian, K. Li, H. Shou, *Plant Biol.* **2010**, *13*, 7–15.
[8] F. Lin, C. L. Lee, S. S. L. Li, T. M. Chu, *Biochemistry* **1983**, *22*, 1055–62.
[9] a) T. R. Anderson, S. U. Toverud, *Arch. Biochem. Biophys.* **1986**, *247*, 131–139; b) A. Hara, H. Sawada, T. Kato, T. Nakayama, H. Yamamoto, Y. Matsumoto, *J. Biochem.* **1984**, *95*, 67–74.
[10] N. Mitić, S. J. Smith, A. Neves, L. W. Guddat, L. R. Gahan, G. Schenk, *Chem. Rev.* **2006**, *106*, 3338–3363.
[11] a) P. Comba, L. R. Gahan, G. R. Hanson, V. Mereacre, C. J. Noble, A. K. Powell, I. Prisecaru, G. Schenk, M. Zajaczkowski-Fischer, *Chem. Eur. J.* **2012**, *18*, 1700–1710; b) G. Schenk, N. Mitic, G. R. Hanson, P. Comba, *Coord. Chem. Rev.* **2013**, *257*, 473–482; c) P. Comba, L. R. Gahan, V. Mereacre, G. R. Hanson, A. K. Powell, G. Schenk, M. Zajaczkowski-Fischer, *Inorg. Chem.* **2012**, *51*, 12195–12209; d) G. Schenk, N. Mitic, L. R. Gahan, D. L. Ollis, R. P. McGeary, L. W. Guddat, *Acc. Chem. Res.* **2012**, *45*, 1593–1603.
[12] a) M. Jarenmark, H. Carlsson, V. M. Trukhan, M. Haukka, S. E. Canton, M. Walczak, W. Fullagar, V. Sundstroem, E. Nordlander, *Inorg. Chem. Commun.* **2010**, *13*, 334–337; b) C. Piovezan, R. Jovito, A. J. Bortoluzzi, H. Terenzi, F. L. Fischer, P. C. Severino, C. T. Pich, G. G. Azzolini, R. A. Peralta, L. M. Rossi, A. Neves, *Inorg. Chem.* **2010**, *49*, 2580–2582; c) A. Neves, M. Lanznaster, A. J. Bortoluzzi, R. A. Peralta, A. Casellato, E. E. Castellano, P. Herrald, M. J. Riley, G. Schenk, *J. Am. Chem. Soc.* **2007**, *129*, 7486–7487; d) M. Lanznaster, A. Neves, A. J. Bortoluzzi, B. Szpoganicz, E. Schwingel, *Inorg. Chem.* **2002**, *41*, 5641–5643; e) A. Neves, M. A. de Brito, V. Drago, K. Griesar, W. Haase, *Inorg. Chim. Acta* **1995**, *237*, 131–135; f) J. J. Danford, P. Dobrowolski, L. M. Berreau, *Inorg. Chem.* **2009**, *48*, 11352–11361; g) C. Belle, I. Gautier-Luneau, L. Karmazin, J.-L. Pierre, S. Albedyhl, B. Krebs, M. Bonin, *Eur. J. Inorg. Chem.* **2002**, 3087–3090; h) S. Albedyhl, M. T. Averbuch-Pouchot, C. Belle, B. Krebs, J. L. Pierre, E. Saint-Aman, S. Torelli, *Eur. J. Inorg. Chem.* **2001**, 1457–1464; i) Y. L. M. Zee, L. R. Gahan, G. Schenk, *Aust. J. Chem.* **2011**, *64*, 258–264; j) A. S. Borovik, V. Papaefthymiou, L. F. Taylor, O. P. Anderson, L. Que Jr., *J. Am. Chem. Soc.* **1989**, *111*, 6183–6195; k) M. Ghiladi, C. J. McKenzie, A. Meier, A. K. Powell, J. Ulstrup, S. Wocadlo, *J. Chem. Soc., Dalton Trans.* **1997**, 4011–4018; l) A. S. Borovik, L. Que Jr., V. Papaefthymiou, E. Muenck, L. F. Taylor, O. P. Anderson, *J. Am. Chem. Soc.* **1988**, *110*, 1986–1988; m) P. Karsten, A. Neves, A. J. Bortoluzzi, M. Lanznaster, V. Drago, *Inorg. Chem.* **2002**, *41*, 4624–4626; n) M. Lanznaster, A. Neves, A. J. Bortoluzzi, V. V. E. Aires, B. Szpoganicz, H. Terenzi, P. C. Severino, J. M. Fuller, S. C. Drew, L. R. Gahan, G. R. Hanson, M. J. Riley, G. Schenk, *J. Biol. Inorg. Chem.* **2005**, *10*, 319–332; o) S. C. Batista, A. Neves, A. J. Bortoluzzi, I. Vencato, R. A. Peralta, B. Szpoganicz, V. V. E. Aires, H. Terenzi, P. C. Severino, *Inorg. Chem. Commun.* **2003**, *6*, 1161–1165; p) F. R. Xavier, A. Neves, A. Casellato, R. A. Peralta, A. J. Bortoluzzi, B. Szpoganicz, P. C. Severino, H. Terenzi, Z. Tomkowicz, S. Ostrovsky, W. Haase, A. Ozarowski, J. Krzystek, J. Telser, G. Schenk, L. R. Gahan, *Inorg. Chem.* **2009**, *48*, 7905–7921; q) F. R. Xavier, R. A. Peralta, A. J. Bortoluzzi, V. Drago, E. E. Castellano, W. Haase, Z. Tomkowicz, A. Neves, *J. Inorg. Biochem.* **2011**, *105*, 1740–1752; r) F. R. Xavier, A. J. Bortoluzzi, A. Neves, *Chem. Biodiversity* **2012**, *9*, 1794–1805.
[13] a) M. Rapta, P. Kamaras, G. B. Jameson, *Polyhedron* **1996**, *15*, 1943–1949; b) C. Belle, I. Gautier-Luneau, G. Gellon, J. L. Pierre, I. Morgenstern-Badarau, E. Saint-Aman, *J. Chem. Soc., Dalton Trans.* **1997**, 3543–3546.
[14] A. Neves, S. M. D. Erthal, V. Drago, K. Griesar, W. Haase, *Inorg. Chim. Acta* **1992**, *197*, 121–124.

[15] a) A. Neves, M. A. de Brito, I. Vencato, V. Drago, K. Griesar, W. Haase, *Inorg. Chem.* **1996**, *35*, 2360–2368; b) H. Adams, D. Bradshaw, D. E. Fenton, *Inorg. Chem. Commun.* **2002**, *5*, 12–14.
[16] a) M. M. E. de Backer, S. McSweeney, P. F. Lindley, E. Hough, *Acta Crystallogr., Sect. D: Biol. Crystallogr.* **2004**, *60*, 1555–1561; b) P. Gettins, J. E. Coleman, *Fed. Proc.* **1982**, *41*, 2966–2973; c) X. Zhang, Y. Zhu, X. Zheng, D. L. Phillips, C. Zhao, *Inorg. Chem.* **2014**, *53*, 3354–3361.
[17] A. Neves, M. A. de Brito, I. Vencato, V. Drago, K. Griesar, W. Haase, *Inorg. Chem.* **1996**, *35*, 2360–2368.
[18] R. T. Paine, Y.-C. Tan, X.-M. Gan, *Inorg. Chem.* **2001**, *40*, 7009–7013.
[19] B. de Souza, G. L. Kreft, T. Bortolotto, H. Terenzi, A. J. Bortoluzzi, E. E. Castellano, R. A. Peralta, J. B. Domingos, A. Neves, *Inorg. Chem.* **2013**, *52*, 3594–3596.
[20] a) R. Sanyal, A. Guha, T. Ghosh, T. K. Mondal, E. Zangrando, D. Das, *Inorg. Chem.* **2014**, *53*, 85–96; b) H. Sakiyama, R. Mochizuki, A. Sugawara, M. Sakamoto, Y. Nishida, M. Yamasaki, *J. Chem. Soc., Dalton Trans.* **1999**, 997–1000; c) J. J. Brown, A. Schöffler, G. Schenk, E. Krenske, L. R. Gahan, unpublished results.
[21] H. Sakiyama, T. Suzuki, K. Ono, R. Ito, Y. Watanabe, M. Yamasaki, M. Mikuriya, *Inorg. Chim. Acta* **2005**, *358*, 1897–1903.
[22] T. Klabunde, N. Strater, R. Frohlich, H. Witzel, B. Krebs, *J. Mol. Biol.* **1996**, *259*, 737–748.
[23] a) A. Neves, M. A. de Brito, I. Vencato, V. Drago, K. Griesar, W. Haase, Y. P. Mascarenhas, *Inorg. Chim. Acta* **1993**, *214*, 5–8; b) A. Kantacha, R. Buchholz, S. J. Smith, G. Schenk, L. R. Gahan, *J. Biol. Inorg. Chem.* **2011**, *16*, 25–32; c) L. J. Daumann, L. Marty, G. Schenk, L. R. Gahan, *Dalton Trans.* **2013**, *42*, 9574–9584; d) L. J. Daumann, K. E. Dalle, G. Schenk, R. P. McGeary, P. V. Bernhardt, D. L. Ollis, L. R. Gahan, *Dalton Trans.* **2012**, *41*, 1695–1708; e) M. Carboni, M. Clemancey, F. Molton, J. Pecaut, C. Lebrun, L. Dubois, G. Blondin, J. M. Latour, *Inorg. Chem.* **2012**, *51*, 10447–10460.
[24] a) E. Safaei, H. Sheykhi, T. Weyhermueller, E. Bill, *Inorg. Chim. Acta* **2012**, *384*, 69–75; b) J. A. Thich, C. C. Ou, D. Powers, B. Vasiliou, D. Mastropaolo, J. A. Potenza, H. J. Schugar, *J. Am. Chem. Soc.* **1976**, *98*, 1425–1433.
[25] L. Borer, L. Thalken, C. Ceccarelli, M. Glick, J. H. Zhang, W. M. Reiff, *Inorg. Chem.* **1983**, *22*, 1719–1724.
[26] G. B. Deacon, R. J. Phillips, *Coord. Chem. Rev.* **1980**, *33*, 227–250.
[27] S. A. Cotton, *Coord. Chem. Rev.* **1972**, *8*, 185–223.
[28] a) C. J. O'Connor, *Prog. Inorg. Chem.* **1982**, *29*, 203–283; b) A. S. Attia, M. F. El-Shahat, *Polyhedron* **2007**, *26*, 791–796; c) J. H. Van Vleck, *The Theory of Electric and Magnetic Susceptibilities*, Oxford University Press, Oxford, **1965**.
[29] a) A. Jozwiuk, A. L. Ingram, D. R. Powell, B. Moubaraki, N. F. Chilton, K. S. Murray, R. P. Houser, *Dalton Trans.* **2014**, *43*, 9740–9753; b) K. K. Nanda, S. K. Dutta, S. Baitalik, K. Venkatsubramanian, K. Nag, *J. Chem. Soc., Dalton Trans.* **1995**, 1239–1244; c) C.-C. Ou, R. A. Lalancette, J. A. Potenza, H. J. Schugar, *J. Am. Chem. Soc.* **1978**, *100*, 2053–2057; d) M. Ghiladi, F. B. Larsen, C. J. McKenzie, I. Sotofte, J.-P. Tuchagues, *Dalton Trans.* **2005**, 1687–1692.
[30] P. J. Hay, J. C. Thibeault, R. Hoffmann, *J. Am. Chem. Soc.* **1975**, *97*, 4884–4899.
[31] I. H. Segel, *Enzyme kinetics: behavior and analysis of rapid equilibrium and steady state enzyme systems*, Wiley-Interscience, New York, **1975**.
[32] C. A. Bunton, S. J. Farber, *J. Org. Chem.* **1969**, *34*, 767–772.
[33] L. R. Gahan, S. J. Smith, A. Neves, G. Schenk, *Eur. J. Inorg. Chem.* **2009**, 2745–2758.
[34] a) R. S. Cox, G. Schenk, N. Mitić, L. R. Gahan, A. C. Hengge, *J. Am. Chem. Soc.* **2007**, *129*, 9550–9551; b) N. Mitic, K. S. Hadler, L. R. Gahan, A. C. Hengge, G. Schenk, *J. Am. Chem. Soc.* **2010**, *132*, 7049–7054.
[35] a) F. Ely, K. S. Hadler, L. R. Gahan, L. W. Guddat, D. L. Ollis, G. Schenk, *Biochem. J.* **2010**, *432*, 565–573; b) F. Ely, K. S. Hadler, N. Mitić, L. R. Gahan, D. L. Ollis, N. M. Plugis, M. T. Russo, J. A. Larrabee, G. Schenk, *J. Biol. Inorg. Chem.* **2011**, *16*, 777–787.
[36] S. Bosch, P. Comba, L. R. Gahan, G. Schenk, *Inorg. Chem.* **2014**, *53*, 9036–9051.
[37] G. Schenk, Y. Ge, L. E. Carrington, C. J. Wynne, I. R. Searle, B. J. Carroll, S. Hamilton, J. de Jersey, *Arch. Biochem. Biophys.* **1999**, *370*, 183–189.
[38] G. M. Sheldrick, T. R. Schneider, *Methods Enzymol.* **1997**, *277*, 319–343.
[39] L. J. Farrugia, *J. Appl. Crystallogr.* **1999**, *32*, 837–838.
[40] a) N. V. Kaminskaia, B. Spingler, S. J. Lippard, *J. Am. Chem. Soc.* **2000**, *122*, 6411–6422; b) L. J. Daumann, P. Comba, J. A. Larrabee, G. Schenk, R. Stranger, G. Cavigliasso, L. R. Gahan, *Inorg. Chem.* **2013**, *52*, 2029–2043; c) T. P. Camargo, F. F. Maia, C. Chaves, B. de Souza, A. J. Bortoluzzi, N. Castilho, T. Bortolotto, H. Terenzi, E. E. Castellano, W. Haase, Z. Tomkowicz, R. A. Peralta, A. Neves, *J. Inorg. Biochem.* **2015**, *146*, 77–88.
[41] M. Maeder, P. King, ed. 1.1, Jplus Consulting Pty Ltd, Perth, Western Australia, **2012**.
[42] B. Das, H. Daver, A. Singh, R. Singh, M. Haukka, S. Demeshko, F. Meyer, G. Lisensky, M. Jarenmark, F. Himo, E. Nordlander, *Eur. J. Inorg. Chem.* **2014**, 2204–2212.
[43] M. Jarenmark, M. Haukka, S. Demeshko, F. Tuczek, L. Zuppiroli, F. Meyer, E. Nordlander, *Inorg. Chem.* **2011**, *50*, 3866–3887.
[44] F. Heims, V. Mereacre, A. Ciancetta, S. Mebs, A. K. Powell, C. Greco, K. Ray, *Eur. J. Inorg. Chem.* **2012**, 4565–4569.

Received: April 1, 2015
Published Online: June 9, 2015

